A Curvilinear Coordinate-Based Split-Step Parabolic Equation Method for Propagation Predictions over Terrain

Ramakrishna Janaswamy, *Senior Member, IEEE*

***Abstract*— Propagation of radiowaves over irregular terrain and in an inhomogeneous atmosphere is solved by the parabolic equation method using the split-step Fourier algorithm on a terrain-conformal mesh. A piecewise continuous coordinate system is generated by the specification of: 1) the terrain profile shape at discrete points and 2) an upper height. The resulting mesh is conformal to the terrain at the lower boundary and gradually flattens off at the maximum height. In addition to preserving the number of points on any vertical line between the terrain and the maximum height from one range step to another, the coordinate transformation used in the paper produces a correction term in the refractive index whose gradient diminishes with height. As a result, the sampling requirements over steep terrain are relaxed when compared to the Beilis–Tappert transformation. Formulation and results are given both for the horizontal and vertical polarizations.**

***Index Terms*—Nonhomogeneous media, propagation.**

I. Introduction

IT is well known that ray bending due to atmospheric inhomogeneities and diffraction due to terrain obstacles play a dominant role in the design of radar or communication systems for frequencies in the very high frequency (VHF) range and above [1]. Although there are several techniques for predicting propagation in such environments, none seem to offer the computational advantages of the parabolic equation (PE) method [2], where one approximates the elliptic operator governing the true wave behavior by a much simpler parabolic operator that permits marching in range. This is especially true in situations where path loss is desired over ranges extending up to a few hundred kilometers and for receiver heights extending up to a few hundred meters. Another advantage of the PE method is its ability to accommodate range-dependent refractive index variations. Of course, the penalty one pays for the simplicity of the PE method is that it neglects backscattering, which is important in some specialized situations such as in clutter modeling and radiowave propagation in highly built-up areas. However, in many propagation problems, one is concerned with gross variations of the signal strength over scales of length that are much larger compared to the wavelength and it is in such regimes that the PE method is expected to play a dominant role. Even where backscattering is important, the results obtained via the PE method prove useful and can be supplemented by other calculations. For example, variations of the signal strength over scales comparable to wavelength occurring in highly built-up urban areas can be handled by statistical means via the Rayleigh fading model [3].

A good introduction to the PE method and its application to radiowave propagation together with the approximations involved is given in [4]. The method has recently been applied by several researchers to radiowave propagation in ducting environments and over terrain [4], [6]–[12]. Of the two schemes available for numerically solving the parabolic equation, viz. the finite-difference and the split-step Fourier technique [5], the latter is clearly more efficient in that it allows much larger height and range step sizes. However, it is more straightforward to implement various boundary conditions at the upper heights with the former than it is with the latter. Levy [7] and Marcus [8] employ the finite-difference technique, while Barrios [9] employs the split-step Fourier technique. It is also possible to use a conformal mapping technique to transform the terrain section between successive range steps into a flat one and solve it numerically [11]. This approach was introduced by Dozier [13] who applied it to acoustic propagation over a rough ocean surface. However, extremely small range steps are needed with the conformal mapping technique making it unattractive to practical problems. In her PE model over terrain, Barrios employs the Beilis–Tappert transformation [10], which creates a family of coordinate lines that are vertical translations of the terrain profile. As a result, the upper boundary is identical in shape to the terrain profile. The consequence of this transformation is that it introduces an additional term in the modified refractive index that increases linearly with height and the rate of this increase is proportional to the curvature of the terrain profile. From a computational perspective, this terrain generated refractive index term places an upper limit on the size of the vertical increment that can be used in the split-step Fourier technique.

In this paper, we solve the standard parabolic equation in an inhomogeneous atmosphere and over irregular terrain by adapting the split-step Fourier technique to a numerically generated mesh. The coordinate transformation to be employed in this paper has previously been applied successfully with the finite-difference technique [15]. The terrain profile data is assumed to be given only at discrete points along the

Manuscript received September 27, 1996; revised February 23, 1998. This work was supported by the Tropospheric Propagation Branch, Division 883, NRaD, San Diego, CA.

The author is with Code EC/Js, Department of Electrical and Computer Engineering, Naval Postgraduate School, Monterey, CA 93943 USA.

Publisher Item Identifier S 0018-926X(98)05789-5.

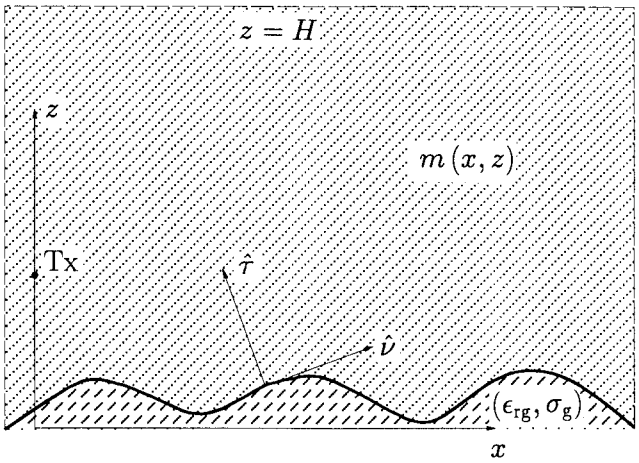

Fig. 1. Propagation over irregular terrain and inhomogeneous atmosphere.

range. A piecewise linear coordinate system is constructed by connecting the terrain points by means of straight lines and generating a family of coordinate lines in the vertical direction that gradually flatten to a Cartesian system at the maximum height. Like the Beilis–Tappert transformation, the presence of sloping terrain produces a correction term in the modified refractive index. However, unlike the former case, the terrain generated correction term has a gradient that gradually diminishes with height and vanishes at the upper height. As a consequence, the present transformation relaxes the sampling requirements over steep terrain while maintaining all of the niceties of the Beilis–Tappert transformation. We present formulation and results both for the horizontal and vertical polarizations. While not the subject matter of the present paper, it is also felt that because the coordinate line flattens and the mesh degenerates into a Cartesian mesh at the top boundary, the present transformation will more readily permit incorporation of any mixed type boundary condition available at a constant height when compared to the Beilis–Tappert transformation.

II. Theory

Fig. 1 shows the geometry of the problem. Given the position of the transmitter (Tx) and the receiver (Rx), the radian frequency ω, the terrain profile, the ground constants $(\epsilon_{\rm rg}, \sigma_{\rm g})$, and the refractive index n of the atmosphere, it is desired to find the loss for the propagation path. The starting point in our formulation is the standard parabolic equation given, for example, in [4]. Assuming an $e^{-i\omega t}$ time dependence, we consider the standard parabolic equation in a medium with parameters (ϵ, μ_0)

$$\frac{\partial U}{\partial x}(x,z) = \frac{i}{2k_0}\frac{\partial^2 U}{\partial z^2}(x,z) + ik_0[m(x,z)-1]U(x,z) \tag{1}$$

where

$$U(x,z) = \begin{cases} \sqrt{r\sin\theta}\, e^{-ik_0 x} E_\phi(r,\theta) \\ \quad \text{for horizontal polarization} \\ \sqrt{\dfrac{r\sin\theta}{\epsilon}}\, e^{-ik_0 x} H_\phi(r,\theta) \\ \quad \text{for vertical polarization} \end{cases} \tag{2}$$

is the reduced field variable and (r,θ,ϕ) are the usual spherical coordinates with origin at the center of the earth. The range and height variables x and z are related to the spherical coordinates via the earth-flattening approximations $x = a_e\theta$ and $z = r - a_e$, where a_e is the radius of the earth. The source is assumed to be located along $\theta = 0$. The quantities E_ϕ and H_ϕ are, respectively, the ϕ components of the electric and magnetic fields. Furthermore, $k_0 = \omega\sqrt{\epsilon_0\mu_0}$ is the free-space wavenumber and

$$m(x,z) = \left(n + \frac{z}{a_e}\right) \tag{3}$$

is the earth-flattened modified refractive index. Given the starting field at $x = 0$, (1) is to be solved subject to an appropriate boundary condition on the ground. For smoothly varying ground having large radius of curvature relative to the wavelength of operation, the behavior of the fields on the ground is approximately governed by the impedance boundary condition $\hat{\tau}\times(\hat{\tau}\times\vec{E}) = -Z_o Z_s \hat{\tau}\times\vec{H}$ [14], where Z_o is the intrinsic impedance of free-space, $\hat{\tau}$ is the unit normal on the terrain surface (see Fig. 1), and Z_s is the normalized surface impedance. The normalized surface impedance is determined from a study of plane wave reflections by the interface. For horizontal polarization, the reflection coefficient for plane waves incident at low grazing angles is close to -1 and it is satisfactory to treat ground as a perfect electric conductor. However, a full impedance boundary condition is necessary for the vertical polarization. The boundary conditions in terms of the U variable are

$$U(x,z) = 0, \quad \text{for horizontal polarization} \tag{4}$$

$$\frac{\partial U}{\partial \tau} + ik_0(Z_s - \sin\nu)U = 0 \quad \text{for vertical polarization.} \tag{5}$$

Note that the $\sin\nu$ term appears in the impedance boundary condition when expressed in terms of the reduced variable U but not in terms of the actual field variable. The normalized surface impedance Z_s depends on the ground constants $(\epsilon_{\rm rg}, \sigma_{\rm g})$ and the angle of incidence of the waves with respect to the normal on the terrain. In this study, we will take Z_s to pertain to horizontally propagating plane waves incident on terrain having a slope angle ν. In this case, the surface impedance becomes

$$Z_s = \frac{\sqrt{\epsilon_{\rm rc} - \cos^2\nu}}{\epsilon_{\rm rc}}. \tag{6}$$

where $\epsilon_{\rm rc}$ is the complex dielectric constant of the ground defined as $\epsilon_{\rm rc} = \epsilon_{\rm rg} + i\sigma_{\rm g}/\omega\epsilon_o \stackrel{\rm def}{=} \epsilon_{\rm rg} + i\sigma_{\rm rg}$.

Equation (1), together with the boundary conditions, constitutes an initial value problem that can be solved numerically by marching along the range variable x to the desired range. As already indicated, we wish to solve the parabolic equation by the split-step Fourier technique [2]. For the purpose of numerical calculations, the domain must first be made finite

by limiting it vertically up to some maximum height H above the reference level. It is assumed that the terrain profile shape is available in a digitized form at several range points along the propagation path. This is the most practical situation. Some coordinate transformation is now required that transforms the region above the uneven terrain into a rectangular one so that one may rigorously implement the split-step Fourier algorithm. If one employs a Cartesian mesh over the uneven terrain, as is suggested in [12], one has to resort to nonphysical approximations such as artificially ignoring field points that fall below the terrain boundary when marching over sloping terrain. We will not pursue that approach here as our objective is to rigorously adapt the split-step algorithm over uneven terrain without introducing additional sources of error.

From a computational standpoint, the following features are desirable of the coordinate transformation.

1) One of the coordinate lines must be conformal to the terrain so that boundary conditions on the terrain can be easily imposed without resorting to interpolation/ extrapolation.
2) The coordinate transformation must introduce as few cross terms as possible in the parabolic equation and the associated boundary condition. This is so that separation of variable technique could be used in the transformed domain.
3) The coordinate transformation must map uniformly spaced points along the vertical in the transformed domain to uniformly spaced points along the vertical in the physical domain. Additionally, the vertical distribution of points in the physical domain must remain the same at the right end of a range step and the left end of the next range step irrespective of the slopes of the terrain in the two range steps; this is not only to permit the use of fast Fourier transforms (FFT's) with uniform sampling, but also to avoid interpolation when using the field computed at one range step as the input for the next range step. The conformal mapping approach of [13], for example, suffers from this deficiency.
4) It is preferable to localize the mesh distortions to the vicinity of the uneven terrain and make the overall mesh as close as possible to a Cartesian mesh in order to reduce the mesh introduced errors in the numerical scheme. This is a well-understood requirement in the finite-difference community. With the split-step technique, this will generally relax the sampling requirements when compared to a uniformly skewed mesh. We will demonstrate this later for the transformation adopted here.
5) Finally, as an added incentive, it is desirable to make the coordinate line at the upper end (mesh truncation point) horizontal so that one could have the potential benefit of incorporating available boundary conditions at a constant height $z = H$. The benefit of using a nonlocal boundary condition at $z = H$ has already been illustrated with the finite-difference technique (e.g., [8]), but is yet to be demonstrated with the split-step Fourier transform technique. We will leave this for future exploration.

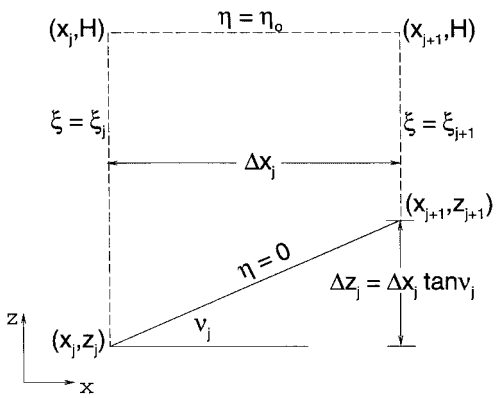

Fig. 2. Coordinate transformation.

Keeping all of the above features in mind, we propose the following transformation for $\xi_j < \xi < \xi_{j+1}, 0 \le \eta \le \eta_0$:

$$x(\xi,\eta) = x(\xi) = x_j + \Delta x_j(\xi - \xi_j) \tag{7}$$

$$z(\xi,\eta) = \left(1 - \frac{\eta}{\eta_0}\right) f[x(\xi)] + \frac{\eta}{\eta_0} H$$

(for terrain described by $z = f(x)$) (8)

$$= \left(1 - \frac{\eta}{\eta_0}\right) [z_j + \Delta z_j(\xi - \xi_j)] + \frac{\eta}{\eta_0} H$$

(for piecewise linear terrain). (9)

where $z = f(x)$ is the equation describing the terrain. In the terrain model used here, we join the discrete data between successive ranges by means of straight lines and directly use (9). The desired coordinate system will map vertical lines into vertical lines and transform the irregular terrain into a flat one. Fig. 2 shows the domain segment between two successive ranges (x_j, x_{j+1}) on a sloping terrain with angle ν_j. Note that ξ and η are dimensionless variables. The terrain boundary corresponds to the map of $\eta = 0$, while the upper boundary $z = H$ to $\eta = \eta_o$. The left and right ends of the segment are generated by $\xi = \xi_j$ and $\xi = \xi_{j+1}$, respectively. The metrics of the transformation within each segment are

$$x_\xi(\xi,\eta) \stackrel{\text{def}}{=} \frac{\partial x}{\partial \xi}(\xi,\eta) = \Delta x_j; \quad z_\xi(\xi,\eta) = \left(1 - \frac{\eta}{\eta_0}\right)\Delta z_j$$

$$x_\eta(\xi,\eta) = 0; \quad z_\eta(\xi,\eta) = \frac{1}{\eta_0}\,[H - z_j - \Delta z_j(\xi - \xi_j)]. \tag{10}$$

Note that while x_ξ, x_η and z_η are continuous across the range step at $\xi = \xi_{j+1}$, z_ξ is discontinuous due to the presence of Δz_j. The transformation defined by (7) and (9) generates a family of coordinate lines $\eta =$ constant, which gradually flatten off at the top with the coordinate line $\eta = 0$ being conformal to the terrain. Such a transformation has the advantage of preserving the number of points at any range step as well as enabling equidistant mesh points along any vertical line. Fig. 3 shows the distribution of coordinate lines on a typical terrain profile. Notice that the distortions of the coordinate lines near the terrain diminish gradually as one approaches the upper boundary. By contrast, the Beilis–Tappert transformation over

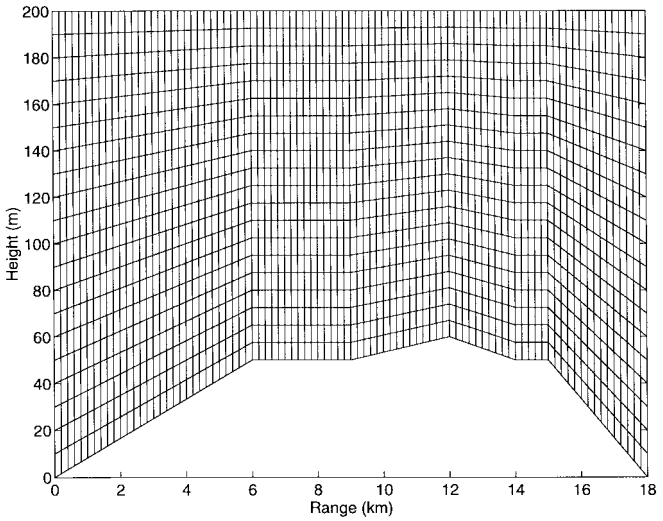

Fig. 3. Curvilinear mesh on a typical terrain.

a terrain will be of the form

$$z(\xi,\eta) = A\eta + f[x(\xi)] \quad \text{(Beilis–Tappert Transformation)} \tag{11}$$

for some scaling constant A. In this case, the distortions of the coordinate lines near the terrain boundary will be carried over indefinitely without change to large heights. The coordinate transformation proposed here will meet all of the desirable features listed previously, whereas the Beilis–Tappert transformation will meet only the first three. Both of the above transformations will introduce a correction term in the refractive index that is dependent on the terrain. However, we will see shortly that while the Beilis–Tappert transformation produces a correction term having a constant gradient with height, the one produced by the transformation (9) diminishes with height and will vanish at the upper boundary. This will have the effect of somewhat relaxing the sampling requirements in the split-step Fourier technique, as we will show later.

Under the transformation (9), the various derivatives become [16]

$$\frac{\partial U}{\partial x} = \frac{1}{x_\xi}\frac{\partial U}{\partial \xi} - \frac{z_\xi}{z_\eta x_\xi}\frac{\partial U}{\partial \eta} \tag{12}$$

$$\frac{\partial U}{\partial z} = \frac{1}{z_\eta}\frac{\partial U}{\partial \eta} \tag{13}$$

$$\frac{\partial^2 U}{\partial z^2} = \frac{1}{z_\eta^2}\frac{\partial^2 U}{\partial \eta^2}. \tag{14}$$

The parabolic equation in (1) gets transformed to

$$\frac{\partial U}{\partial \xi} = \frac{z_\xi}{z_\eta}\frac{\partial U}{\partial \eta} + i\,\frac{x_\xi}{2k_0 z_\eta^2}\frac{\partial^2 U}{\partial \eta^2} + ik_0 x_\xi[m(\xi,\eta)-1]U \tag{15}$$

and the boundary conditions become

$$U(\xi,\eta=0) = 0, \quad \text{(horizontal polarization)} \tag{16}$$

$$\frac{\partial U}{\partial \eta} - \frac{i\tan\nu_j}{2k_0 z_\eta}\frac{\partial^2 U}{\partial \eta^2} + ik_0\frac{z_\eta}{\cos\nu_j}(Z_s - \sin\nu_j)\,U = 0 \quad (\text{at } \eta = 0, \text{vertical polarization}). \tag{17}$$

Because the normal derivative on the ground involves both $\partial/\partial\xi$ and $\partial/\partial\eta$, the boundary condition for vertical polarization would involve both of these derivatives. In deriving (17), we made use of the parabolic equation in (15) to eliminate $\partial U/\partial\xi$ and substituted $m(\xi,\eta=0)\approx 1$ on the terrain. It is seen that the presence of a sloping terrain $(\nu_j \neq 0)$ results in an additional term $\partial U/\partial\eta$ in the parabolic equation and $\partial^2 U/\partial\eta^2$ in the boundary condition for vertical polarization. It is to be noted that the boundary condition in (17) is inhomogeneous in the sense that the coefficients are functions of ξ. This is in contrast to the flat earth case where the coefficients are all constant.

Presence of the term involving the first partial derivative $\partial U/\partial\eta$ on the right-hand side of (15) will not allow a solution in terms of Fourier transforms. This is because functions of the form $\sin\lambda\eta$ or $\cos\lambda\eta$ are no longer the eigenfunctions of the right-hand side operator of (15). To get rid of the first derivative term, we will employ the trick used in [10] and define a new field variable V

$$V(\xi,\eta) = U(\xi,\eta)e^{(i/2)k_0 z_\eta(\xi)\eta_0\tan\nu(1-\eta/\eta_0)^2} \qquad \xi_j \le \xi < \xi_{j+1} \tag{18}$$

which differs from the original field variable through the exponential factor. The argument of the exponential function has been chosen so as to cancel off the $\partial/\partial\eta$ term. The PE in terms of the new field variable will be modified to

$$\frac{\partial V}{\partial \xi} = i\,\frac{x_\xi}{2k_0 z_\eta^2}\frac{\partial^2 V}{\partial \eta^2} + \left[\frac{x_\xi\tan\nu}{2z_\eta\eta_o} + ik_0 x_\xi(m-1)\right]V \tag{19}$$

$$\stackrel{\text{def}}{=} Q(\xi,\eta)V \tag{20}$$

where $Q(\xi,\eta)$ is the differential operator representing the right-hand side of (19). For slowly varying refractive index profiles, (20) may be solved in an operator form as

$$V(\xi_{j+1}^-,\eta) = e^{\overline{Q}_j(\eta)}\,V(\xi_j^+,\eta) \tag{21}$$

where the superscripts $-$ and $+$ denote values to the left of and to the right of, respectively, and

$$\overline{Q}_j(\eta) = \int_{\xi=\xi_j}^{\xi_{j+1}} Q(\xi,\eta)\,d\xi \tag{22}$$

is the average of the operator Q over the jth range step. Substituting (10) into (22), the averaged operator can be obtained as (defining the height increment at $\xi = \xi_j$ as $h_j = (H - z_j)/\eta_0$)

$$\overline{Q}_j(\eta) = ik_0 x_\xi\left[\frac{1}{2k_0^2 h_j h_{j+1}}\frac{\partial^2}{\partial\eta^2} + \overline{m}^j - 1\right] + \frac{1}{2}\ln\left[\frac{h_j}{h_{j+1}}\right] \tag{23}$$

where

$$\overline{m}^j(\eta) = \int_{\xi=\xi_j}^{\xi_{j+1}} m(\xi,\eta)\,d\xi \tag{24}$$

is the average value of the modified refractive index over the jth range step. Relating the new field V at the left and right

of $\xi = \xi_{j+1}$ through (18), the final solution in terms of the function V is then

$$V(\xi_{j+1},\eta) = \sqrt{\frac{h_j}{h_{j+1}}}\; e^{ik_0 x_\xi(\overline{m}^j_{\rm ter}-1)}\; e^{i(x_\xi/2k_0h_jh_{j+1})(\partial^2/\partial\eta^2)} \cdot [V(\xi_j,\eta)] \tag{25}$$

where $\overline{m}^j_{\rm ter}$ is the terrain modified, effective refractive index over the jth segment and is given by

$$\overline{m}^j_{\rm ter} = \overline{m}^j + \frac{\eta_0 h_{j+1}}{2x_\xi}\;(\tan\nu_{j+1} - \tan\nu_j)\left(1-\frac{\eta}{\eta_0}\right)^2. \tag{26}$$

It is seen that the effect of the terrain is to: 1) introduce an extra term in the modified refractive index that is dependent on the difference of slopes (or *finite curvature*, for want of better terminology); this term goes to zero at the upper end $\eta = \eta_0$ and 2) a gain (loss) factor for up-slope (down-slope) terrain. This is in contrast to the Beilis–Tappert transformation which will produce a terrain modified refractive index of (in our notation)

$$\overline{m}^j_{\rm ter} = \overline{m}^j + A\eta\,\frac{d^2f(x)}{dx^2} \quad \text{(Beilis–Tappert transformation).} \tag{27}$$

In this case, the terrain introduced refractive index term increases uniformly with height and the rate of increase is proportional to the curvature of the terrain.

It now remains to define an appropriate Fourier transform to represent the exponential operator in (25) to complete the solution. It may be noted at the outset that the terrain dependent term in (26) will place a lower limit on the sampling rate required to represent the field on any vertical line.

Horizontal polarization with the Dirichlet boundary condition poses no difficulty and we use the usual sine transforms. However, vertical polarization with the Robin-type boundary condition deserves special attention. Before we express the boundary condition in terms of the V function, we will make some approximations.

Because it is not straightforward to incorporate the second derivative term present in the boundary condition (17) into the split-step algorithm, we will ignore it altogether. To assess the extent of errors caused by this approximation, we assume an elementary solution of the form

$$U = e^{-ik_0x}e^{ik_0(x\cos\beta + z\sin\beta)}$$

and compare the contribution due to the second derivative term to the overall contribution. The second derivative term can be ignored provided that

$$|\sin\beta\tan\nu_j| \ll 2$$

which will be satisfied for

$$\tan|\nu|_{\max}\sin\beta_{\max} \ll 2 \tag{28}$$

where $\beta_{\max}$ and $|\nu|_{\max}$ are the maximum propagation and the maximum absolute terrain angles, respectively. As an example, for a maximum propagation angle of 15° and a maximum terrain angle of 30°, the left-hand side is approximately 0.15, which is $\ll 2$. The above condition is always satisfied for terrain problems that can be handled with the standard parabolic equation. Making use of the relation (18) between U and V, the simplified boundary condition in terms of the modified field variable V is

$$\frac{\partial V}{\partial\eta} + ik_0 z_\eta(\xi) Z_s \sec\nu V = 0.$$

The metric $z_\eta(\xi)$ present in the second term varies linearly over the jth range step $\xi_j \le \xi \le \xi_{j+1}$. It takes a value of h_j at the left end ($\xi = \xi_j$) and h_{j+1} at the right end ($\xi = \xi_{j+1}$), which are, respectively, the height increments at the left end and the right end. The quantity can be replaced with the average height increment over the jth range step $h^{\rm ave}_j = (h_j + h_{j+1})/2$ provided that the difference between h_j and h_{j+1} be a small fraction of $h^{\rm ave}_j$, viz.

$$|h_j - h_{j+1}| \ll \frac{1}{2}\,(h_j + h_{j+1}) \Rightarrow H - \frac{z_j + z_{j+1}}{2} \;\gg |\Delta z_j| \tag{29}$$

which suggests that the height of the upper boundary about the average terrain height must be large compared to the change in terrain height over the range step. In the current implementations of the split-step algorithm, where no special treatment at the upper boundary is made, the height is often chosen very large—well beyond the above stipulation—so that errors due to artificial truncation at the upper end are not severe. Equation (29) is automatically satisfied most of the time. In practice, one may get by with replacing $\gg$ by ≥ 5. The approximate boundary condition for vertical polarization subject to (28) and (29) is then

$$\frac{\partial V}{\partial\eta} + ik_0 h^{\rm ave}_j Z_s \sec\nu_j V = 0. \tag{30}$$

By comparing with the boundary condition over flat terrain in [4], we see that the primary effect of sloping terrain is to result in an effective surface impedance equal to $\sec\nu_j Z_s$. For $\nu_j = 0$ and the surface impedance is $Z_s = \sqrt{\epsilon_{\rm rc}-1}/\epsilon_{\rm rc}$, whereas for $\nu_j \ne 0$, the effective surface impedance $Z_s\,\sec\nu_j = \sqrt{\sec^2\nu_j\,\epsilon_{\rm rc}-1}/\epsilon_{\rm rc}$. At this point it should be straightforward to use the discrete mixed Fourier transforms put forth by Dockery and Kuttler [17] to result in an optimized code for vertical polarization. However, we present a formulation based on continuous Fourier transforms in this paper. Using complex exponentials, the Fourier transform relations for vertical polarization can be obtained in a manner similar to that presented in [4] as

$$V(\xi_j,\eta) = \frac{1}{2\pi}\int_0^\infty \left[\frac{e^{-ip\eta}}{p-\alpha_j} + \frac{e^{ip\eta}}{p+\alpha_j}\right]\tilde{V}(\xi_j,p)\,dp + S\,e^{-i\alpha_j\eta} \tag{31}$$

$$\tilde{V}(\xi_j,p) = \int_0^\infty [(p-\alpha_j)e^{ip\eta} + (p+\alpha_j)e^{-ip\eta}]V(\xi_j,\eta)\,d\eta \tag{32}$$

$$S = 2i\alpha_j\int_0^\infty V(\xi_j,\eta)e^{-i\alpha_j\eta}\,d\eta \tag{33}$$

where $\alpha_j = k_0 h_j^{\text{ave}} \sec \nu_j Z_s$. The above forms presented are identical mathematically to those given in [4]. We prefer to cast the equations in the complex exponential form to enable us to directly use complex FFT routines. The last term present in the inverse transform formula in (31) denotes a surface wave and may be ignored for frequencies exceeding a few tens of MHz [4]. Having defined the necessary Fourier transforms, the solution in (25) can be completed by recognizing that $e^{\partial^2/\partial\eta^2}[e^{iq\eta}] = e^{-q^2} \cdot e^{iq\eta}$. This is true of each of the individual terms in (31).

III. Numerical Results

To contain the computational domain vertically in the physical space (to the maximum height H) and to bandlimit the signal in the p space, we use a Hanning window in the respective domains. The required Fourier transforms are all evaluated by means of an N-point complex FFT. There are two factors that will influence sampling of the field in the vertical direction:

1) the maximum propagation angle $\beta_{\max}$ with respect to the horizontal;
2) the maximum of the absolute terrain slope angle $|\nu|_{\max}$; this is a consequence of the correction introduced into the modified refractive index due to a variable slope terrain as evidenced in (26).

We choose increments in the transformed coordinates to be $\Delta\xi = 1 = \Delta\eta$. The phase shift per vertical increment for a plane wave traveling at an angle β with respect to the horizontal is $k_0 h_j \sin\beta$ and may be identified with the Fourier transform variable p in (31) and (32). Now

$$p_{\max} = \max_j \{k_0 h_j \sin\beta\} \stackrel{\text{def}}{=} k_0 \Delta z_{\max} \sin\beta_{\max} \tag{34}$$

where $\Delta z_{\max}$ is the maximum vertical increment over the entire computational domain.

From (25) and (26), the additional phase Φ_j (or phase distortion) introduced by the uneven terrain is

$$\Phi_j = k_0 h_{j+1} (\tan\nu_{j+1} - \tan\nu_j) \frac{\eta_0}{2} \left(1 - \frac{\eta}{\eta_0}\right)^2.$$

This phase has a maximum value at the terrain and decreases quadratically to zero at the upper end. It is the rate of change of phase that dictates sampling in the vertical direction. The rate of change of phase is

$$\frac{d\Phi_j}{d\eta} = -k_0 h_{j+1} (\tan\nu_{j+1} - \tan\nu_j)\left(1 - \frac{\eta}{\eta_0}\right)$$

which vanishes at the upper end $\eta = \eta_o$. A very conservative estimate for the sampling can be made based on the *maximum* rate of change of phase. However, because the phase distortion introduced by the transformation decrease with height and goes to zero at the upper end, we have observed that a somewhat less conservative estimate may be made based on the *average* rate of change of phase. The absolute value of the average rate of change of phase is

$$\begin{aligned}\left|\frac{d\Phi_j}{d\eta}\right|_{\text{ave}} &= k_0 h_{j+1} |\tan\nu_{j+1} - \tan\nu_j| \\ &\quad \left|\frac{1}{\eta_0}\int_0^{\eta_0} \left(1 - \frac{\eta}{\eta_0}\right) d\eta\right| \\ &= \frac{k_0 h_{j+1}}{2} |\tan\nu_{j+1} - \tan\nu_j| \\ &\le k_0 \Delta z_{\max} \tan|\nu|_{\max} \\ &\stackrel{\text{def}}{=} \Delta\Phi_{\max}^{\text{ave}}.\end{aligned}$$

To prevent aliasing, we require by sampling theorem that $p_{\max}, \Delta\Phi_{\max}^{\text{ave}} \le \pi$. From the above we get

$$\Delta z_{\max} \le \frac{\lambda_0}{2} \min\left\{\frac{1}{\sin\beta_{\max}}, \frac{1}{\tan|\nu|_{\max}}\right\} \tag{35}$$

where λ_0 is the wavelength in free-space. Hence, for shallow terrain (small $|\nu|_{\max}$), field sampling in the vertical direction is governed by the maximum propagation angle chosen, whereas over steep terrain, it is governed by the maximum terrain slope angle. A similar analysis performed on the Beilis–Tappert transformation reveals that

$$\Delta z_{\max} \le \frac{\lambda_0}{2} \min\left\{\frac{1}{\sin\beta_{\max}}, \frac{1}{2\tan|\nu|_{\max}}\right\}$$
(Beilis–Tappert transformation).

Hence, for terrain-dominated field sampling, Beilis–Tappert transformation requires twice as many points in the vertical direction as the present approach. This is due to the fact that the terrain introduced phase distortion remains the same at all heights with Beilis–Tappert transformation in contrast to the transformation (9).

To better appreciate the simplicity and ease of implementing the present algorithm, we outline the steps needed to perform field computations given the frequency of operation, the initial field, digitized terrain data $(x_k, z_k), k = 1, \cdots, K$, a nominal range increment Δx, the maximum height H, the maximum propagation angle $\beta_{\max}$, the modified refractive index $m(x, z)$, and the ground constants $(\epsilon_{rg}, \sigma_g)$.

1) Assume straight-line interpolation between the given points $(x_k, z_k), k = 1 \cdots, K$. Generate additional points between (x_k, z_k) and (x_{k+1}, z_{k+1}) to within the range resolution if the horizontal separation between them is significantly greater than the desired range resolution Δx. Thus, we generate the points $(x_j, z_j), j = 1, \cdots, J$ with $J \ge K$ such that $x_{j+1} - x_j = \Delta x_j \approx \Delta x$. The total number of range steps equals $J - 1$.
2) Compute $\tan\nu_j = (z_{j+1} - z_j)/\Delta x_j, j = 1, \cdots, J-1$ and determine $\tan|\nu|_{\max}$.
3) Estimate $\Delta z_{\max}$ from (35) and determine the complex FFT size
$$N \sim 2 \max_j \left[\frac{H - z_j}{\Delta z_{\max}}\right]$$
where $\sim$ is the nearest modulo-two integer corresponding the the right-hand side. The constant $\eta_o = N/2$.
4) Compute $h_j = (H - z_j)/\eta_o, j = 1, \cdots, J$.

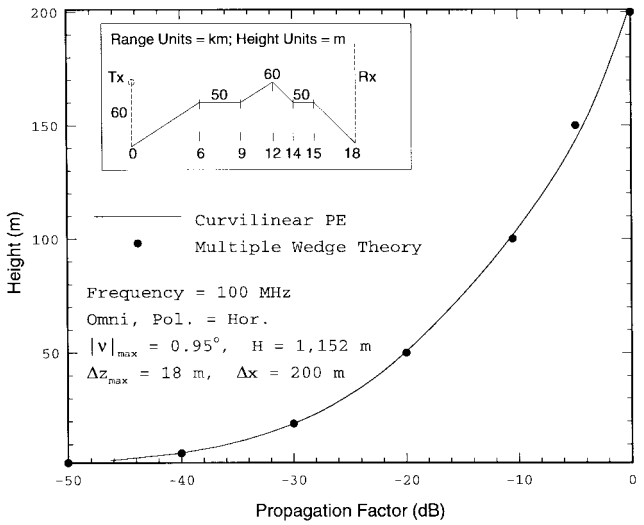

Fig. 4. Propagation over perfectly conducting wedges.

5) Using the appropriate transform relationships (i.e., sine transforms for horizontal polarization or (31)–(33) for vertical polarization) perform the transform of the field $V(\xi_j, \eta)$ at the initial range $\xi = \xi_j$, propagate in free-space over Δx_j and get the inverse transform. Multiply the spatial field with $\sqrt{h_j/h_{j+1}}$ to get the true field $|V(\xi_{j+1}, \eta)|$ at the new range $\xi = \xi_{j+1}$. Noting that $|U(\xi, \eta)| = |V(\xi, \eta)|$, obtain the propagation factor at the new range.
6) Make phase corrections to the spatial field obtained in step 5) by multiplying with $e^{-jk_0\Delta x_j(\overline{m}_j^{\text{tor}}-1)}$. Increment j and repeat step 5) to exhaust all range steps.

Compared to propagation over flat terrain, the primary computational burden presented by uneven terrain in the split-step algorithm is the extra multiplication in step 6) for phase correction. This extra operation, of order $O(N)$ will also be present with the Beilis–Tappert transformation. The computational time with uneven terrain will still be of order $O(N \log N)$ and the overhead introduced by the terrain is not detrimental to the efficiency of the overall algorithm. Maintaining all of the niceties, the present approach presents an advantage over the Beilis–Tappert transformation in that it requires half as many FFT points as the latter.

In what follows, we will present results for the propagation factor PF or path loss PL for a dipole source of field moment $U_o\ell$, where U_o is some arbitrary constant having the same dimensions as the field variable U and ℓ is the length of the dipole. The propagation factor (which is defined as the excess signal strength over free-space) for a dipole with a *unit-field moment* (in free-space the dipole source produces a field, which, under the paraxial approximation, has a magnitude $|U_o\ell|/\sqrt{x\lambda_0}$ at range x) is

$$PF = 10\log(|U|^2 x\lambda_0)$$

and is related to path loss via

$$PL = 20\log\left(\frac{4\pi x}{\lambda_0}\right) - PF.$$

The first example we consider is that of propagation over a shallow terrain comprised of wedges. A horizontally polarized antenna operating at 100 MHz is located at a height of 60 m over a perfectly conducting, hilly terrain whose profile is shown in the inset in Fig. 4. The PE solution is compared with a higher order UTD wedge diffraction theory recently put forth by Holm [18]. The maximum terrain slope angle is less than 1° and we have chosen to include propagation angles up to ±5°. In this example, $\Delta z_{\max}$ is limited by the maximum propagation angle. Propagation factor is determined at a range of 18 km. A refractive index of unity has been chosen for the atmosphere and other parameters for PE marching are indicated on the figure. An excellent agreement with the multiple wedge diffraction theory is seen.

We next choose propagation over a steep triangular hill having a base angle of around 27° (Fig. 5). A horizontally polarized source is located at zero range and height of 100 m and the field is computed at a range of 15 km. The frequency of operation is 1 GHz and the hill is about 670 wavelengths high. The PE results are compared with a four-ray knife-edge theory [19], [20], which accounts for reflections between the transmitter and hill and the hill and receiver. In this case, $\Delta z_{\max}$ is limited to a wavelength by the rather high-terrain slope angle. Although it is not obvious from the figure, the maxima between the two results in the highly oscillatory, shadow region behind the hill differ by less than 2 dB. An excellent agreement with the knife-edge diffraction theory is seen for all heights up to 460 m. Although this example seems to suggest that we are forced to use a small vertical increment for large terrain angles, it is interesting to note that practically identical results were obtained when the slope angle was reduced to 10°, while maintaining the height of the triangular hill constant. It may be noted that the knife-edge diffraction results are for a vertical knife edge which has a slope angle of 90°! The good agreement between the two is due to the fact that large propagation angles are not involved in the above example at the range of 15 km. Hence, in regions of low propagation angles, a shallower approximation of a steep terrain should be permissible in the PE modeling. Of course, we do not expect the above argument to be valid very close to the knife edge where high-propagation angles will be involved.

Next, we consider propagation of a vertically polarized source over a valley (Fig. 6). The slope angle of each wall is ±5.7° and the front edge of the valley is located 30 km from the source. The source operates at 100 MHz and is situated on the ground. The ground is characterized by $\epsilon_{rg} = 4, \sigma_g = 1$ mS/m, which pertain to very dry soil. Standard atmospheric condition has been assumed ($M = [m-1] \times 10^6 = 0.118\, z$, where z is in meters). This example was considered by Marcus [8] in his finite-difference approach (IFDG equation). Path loss is computed at the center of the valley where our mesh will be most sparsely spaced. In this example, we choose a maximum propagation angle of about 10° (this is suggested by observing the data of [8] deep within the valley) and a $\Delta z_{\max} = 6.4$ m $\approx 2\lambda_0$ (actually good results were obtained when $\Delta z_{\max} = 9$ m was used as suggested by (35). We included finer sampling to show a smoother variation of field in the plots). The range increment is once again $\Delta x = 200$ m. It is seen the results

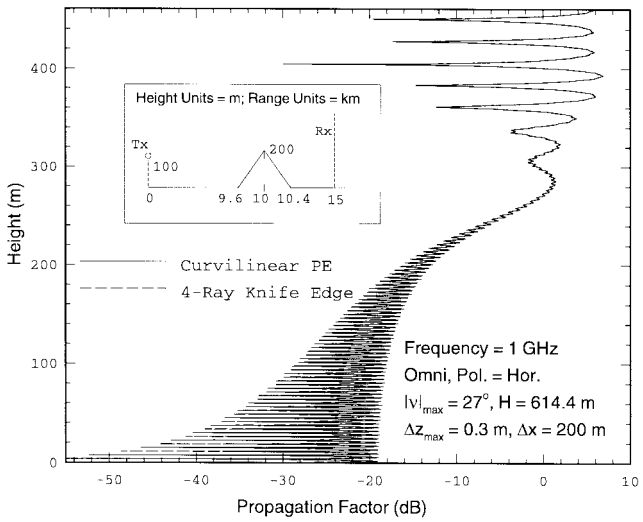

Fig. 5. Propagation over a steep triangular hill.

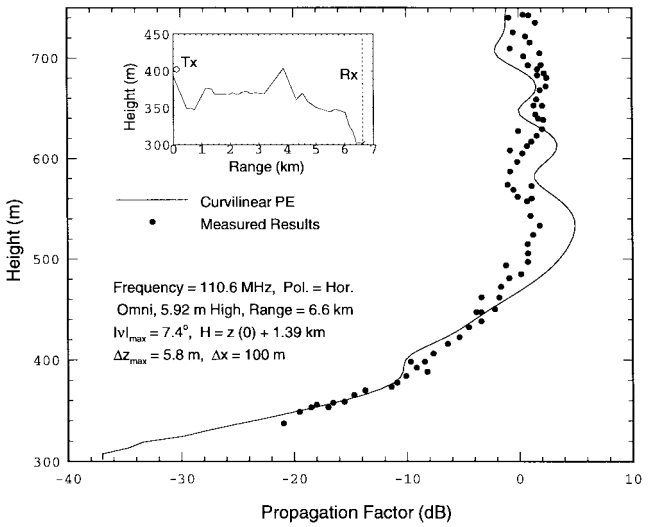

Fig. 7. Propagation factor versus height for Natty Pond site.

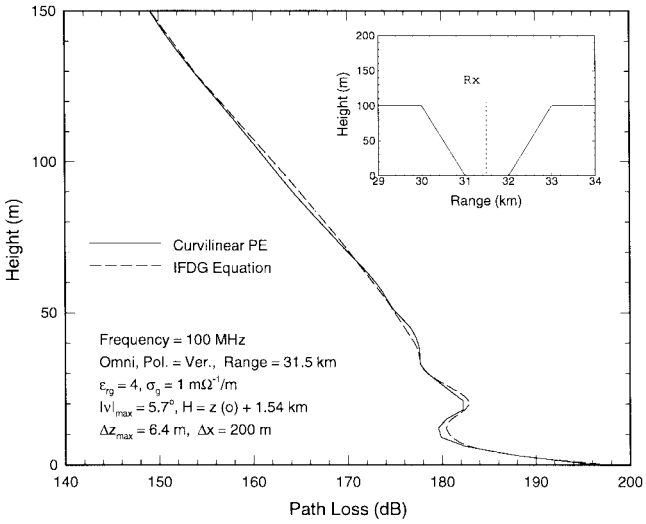

Fig. 6. Path loss over a valley for vertical polarization.

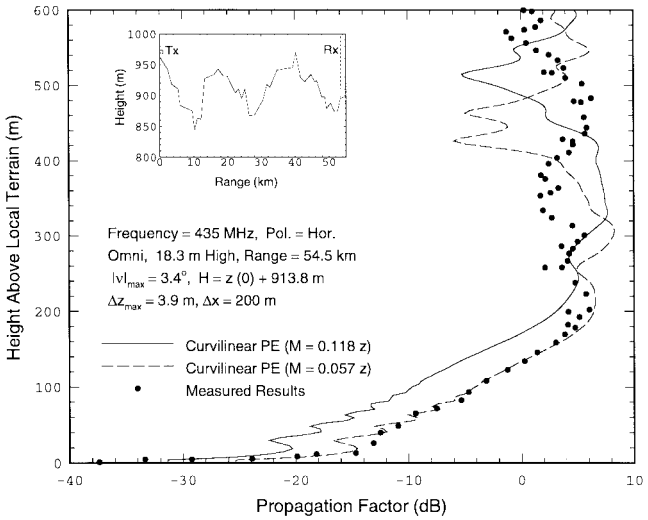

Fig. 8. Propagation factor versus height for Beiseker site.

compare very well with those of Marcus who used $\Delta z_{\max} = 1$ m and $\Delta x = 1$ m within the valley. This example also brings out clearly the computational advantages of the split-step algorithm over the finite-difference approach. We have also observed, in this example, that the results obtained with and without the surface waves in (31) were within 0.2 dB of each other.

We have also validated our numerical results with measured results available in the literature. Meeks [21] presented data on VHF measurements at low altitudes over hilly forested terrain taken in Gardner, MA. The frequency of operation was 110.6 MHz with a ring of horizontally polarized loop antennas placed one half-wavelength above a conducting ground plane located 4.6 m above the local terrain. The terrain profile is shown in the inset in Fig. 7. From the terrain data provided, we compute the maximum slope angle as 7.4°. Choosing a maximum propagation angle of 10°, we obtain a maximum height increment of $\Delta z_{\max} = 5.8\,\text{m} \approx 2\lambda_0$. A range increment of $\Delta x = 100$ m (the range resolution of the digitized data was 133 m) is picked. A standard atmosphere is chosen for the environmental data. Propagation factor is calculated and compared at a range of 6.6 km. The comparison is shown in Fig. 7. Knife-edge diffraction effects are clearly seen in the deep shadow region in both the computed and measured results. A very good agreement with measured data is seen. At this rather short range of 6.6 km and low frequency of 110.6 MHz, refractive index variations will have a minimal effect on the results. This was actually verified by setting $m = 1$ and repeating the PE computations. No noticeable change in the results was obtained.

We show a final comparison with measured results, this time at a higher frequency and a much longer range. Propagation measurements were made by Massachusetts Institute of Technology (MIT) Lincoln Laboratory, Cambridge, MA, over several sites in Canada. We show comparison of our results for the Beiseker area in Alberta, Canada. Measurements were carried out with a horizontally polarized transmitting antenna operating at 435 MHz and located at a height of 18.3 m above the local terrain. The receiver was placed at a range of 54.5 km. The terrain profile is shown in the inset in Fig. 8.

The maximum slope angle for the terrain in this example is 3.4°. We choose $\beta_{max} = 5°$ to yield $\Delta z_{\max} = 3.9$ m. The range increment chosen is $\Delta x = 200$ m. Two computations were performed with the PE formulation: one using a standard atmosphere having $M = 0.118\ z$ and a second using super-refractive atmosphere having $M = 0.057\ z$. The propagation factor at this long range is expected to be sensitive to the refractive index profile. This is clearly seen in Fig. 8. The measured results are generally in good agreement with both of these results, although a better agreement is obtained with the latter. The differences seen between the numerical and measured results are attributed to the lack of proper environmental data.

IV. Conclusion

The standard parabolic equation was transformed and solved using the split-step algorithm in a curvilinear coordinate system to permit accurate modeling over terrain. The curvilinear mesh is very easy to generate, dictated only by the digitized data of the terrain and a maximum height for field computation. The coordinate lines are conformal to the terrain at the lower boundary and gradually flatten at the upper end. The present transformation has the advantage of preserving the number of points on any vertical line between the terrain and a constant upper height. It produces a correction term to the refractive index whose gradient diminishes at the upper end. Formulation was given both for the horizontal and vertical polarizations and the numerical results were validated by showing comparisons with other approaches and measured results.

It was shown that the field sampling in the vertical direction depends not only on the maximum propagation angle, but also on the maximum slope angle of the terrain. A higher slope angle would, in general, require a finer mesh in the vertical direction. However, compared to the Beilis–Tappert transformation, a larger vertical increment can be used with the present transformation. It is also felt that at least over regions reachable by low propagation angles, one may approximate a steep terrain by a reasonably shallow terrain and still get meaningful results.

Because the curvilinear mesh degenerates into a rectangular one at the upper end, it is felt that it would be easier to implement more sophisticated boundary conditions at the upper end in conjunction with the split-step algorithm using the present transformation than possible with previous transformations. Although yet to be demonstrated, this could have the potential of better containing the computational domain in the vertical direction than presently possible. This will be investigated in the future.

Acknowledgment

The author would like to thank Dr. S. Marcus of RAFAEL, Haifa, Israel, for providing the IFDG data shown in Fig. 6 and A. E. Barrios of NRaD, San Diego, CA, for providing the measured results shown in Figs. 7 and 8. The author would also like to thank H. V. Hitney of NRaD, San Diego, CA, for providing encouragement in carrying out the present work.

References

[1] D. E. Kerr, Ed., *Propagation of Short Radiowaves*. London, U.K.: Peter Peregrinus Ltd., 1980.
[2] F. D. Tappert, "The parabolic approximation method," in *Wave Propagation and Underwater Acoustics* (lecture notes in physics), J. B. Keller and J. S. Papadakis, Eds. New York: Springer-Verlag, vol. 70, 1977.
[3] J. D. Parsons, *The Mobile Radio Propagation Channel*. London, U.K.: Pentech, 1992.
[4] J. R. Kuttler and G. D. Dockery, "Theoretical description of the parabolic approximation/Fourier split-step method of representing electromagnetic propagation in the troposphere," *Radio Sci.*, vol. 26, no. 2, pp. 381–393, Mar./Apr. 1991.
[5] F. B. Jensen, W. A. Kuperman, M. B. Porter, and H. Schmidt, *Computational Ocean Acoustics*. New York: Amer. Inst. Phys. (AIP), 1994, ch. 6.
[6] K. H. Craig and M. F. Levy, "Parabolic equation modeling of the effects of multipath and ducting on radar systems," *Proc. Inst. Elect. Eng.*, vol 138, pt. F, pp. 153–162, 1991.
[7] M. F. Levy, "Parabolic equation modeling of propagation over irregular terrain," *Electron. Lett.*, vol. 26, no. 15, pp. 1153–1155, July 1990.
[8] S. H. Marcus, "A hybrid (finite-difference surface Green's function) method for computing transmission losses in an inhomogeneous atmosphere over irregular terrain," *IEEE Trans. Antennas Propagat.*, vol. 40, pp. 1451–1458, Dec. 1992.
[9] A. E. Barrios, "A terrain parabolic equation model for propagation in the troposhpere," *IEEE Trans. Antennas Propagat.*, vol. 42, pp. 90–98, Jan. 1994.
[10] A. Beilis and F. D. Tappert, "Coupled mode analysis of multiple rough surface scattering," *J. Acoust. Soc. Amer.*, vol. 66, no. 3, pp. 811–826, Sept. 1979.
[11] K. Vlachos, "A wide angle split-step parabolic equation model for propagation predictions over terrain," M.S.E.E. thesis, Naval Postgraduate School, Monterey, CA, Mar. 1996.
[12] A. E. Barrios, "Terrain and refractivity effects on nonoptical paths," in *AGARD Conf. Proc. 543—Meet. Multiple Propagat. Paths*, The Netherlands, Oct. 1993, pp. 10.1–10.9.
[13] B. L. Dozier, "PERUSE: A numerical treatment of rough surface scattering for the parabolic wave equation," *J. Acoust. Soc. Amer.*, vol. 75, no. 5, pp. 1415–1432, 1982.
[14] T. B. A. Senior, "Impedance boundary conditions for imperfectly conducting surfaces," *Appl. Sci. Res.*, vol. 8, no. B, pp. 419–436, 1960.
[15] J-K Lee, "Radiowave propagation over an irregular terrain using the parabolic equation method in a curvilinear coordinate system," M.S.E.E. thesis, Naval Postgraduate School, Monterey, CA, Mar. 1995.
[16] J. F. Thompson, Z. U. A. Warsi, and C. W. Mastin, *Numerical Grid Generation*. New York: North-Holland, 1985.
[17] G. D. Dockery and J. R. Kuttler, "An improved impedance boundary algorithm for Fourier split-step solutions of the parabolic wave equation," *IEEE Trans. Antennas Propagat.*, vol. 44, pp. 1592–1599, Dec. 1996.
[18] P. D. Holm, "UTD-diffraction coefficients for higher order wedge diffracted fields," *IEEE Trans. Antennas Propagat.*, vol. 44, pp. 879–888, June 1996.
[19] M. L. Meeks, *Radar Propagation at Low Altitudes*. Dedham, MA: Artech House, 1982.
[20] L. J. Anderson and L. G. Trolese, "Simplified method for computing knife edge diffraction in the shadow region," *IRE Trans. Antennas Propagat.*, vol. 6, pp. 281–286, July 1958.
[21] M. L. Meeks, "VHF Propagation over hilly forested terrain," *IEEE Trans. Antennas Propagat.*, vol. AP-31, pp. 483–489, May 1983.
[22] S. Ayasli, "SEKE: A computer model for low altitude radara propagation over irregular terrain," *IEEE Trans. Antennas Propagat.*, vol. AP-34, pp. 1013–1023, Aug. 1986.

Ramakrishna Janaswamy (S'82–M'83–SM'93), for a photograph and biography, see p. 1591 of the November 1997 issue of this Transactions.